Preliminary Design and Analysis of an Unmanned Aerial Vehicle Wing

Created by:
Austin Beine
David Bushnell
Eric Stewart
Bradley Torgler

May 12, 2004
Spring 2004

Prepared for
Dr. Richard Hale
Associate Professor
University of Kansas

Table of Contents

List of Figures

6.6 Upper Stringer Crippling / Buckling

When the analysis of the stringers (both top and bottom) was conducted, several initial assumptions were made. First, it was assumed that all of the stringers would be loaded axially, and that the upper stringers would be loaded in compression only and that the lower stringers would only be subjected to tensile loads. Secondly, it was assumed that all of the material properties of the stringers would be based on the LT material type of Military Handbook 5. Third, a factor of safety of 1.5 was multiplied into the limit load taken from the FEM in order to calculate the margins of safety for the ultimate load on the system. Finally, it was assumed that the upper stringers must not fail in crippling or buckling at the limit load.

Before values were collected from the PATRAN model, several calculations needed to be conducted in order to determine the critical buckling and crippling loads for the stringers when the stringers are under compressive loads. These calculations are based on the following material properties for the stringers:

1) The stringers are standard UL #3 extrusions.
2) The stringers are made of 2024-T3 extrusions.
3) The number of stringers varies based on the wing station location along the wing (there are two stringers on the top skin and one stringer on the bottom skin at wing stations 180-216, three stringers along the top skin and two stringers along the bottom skin at wing stations 120-180, and four stringers along the top skin and three stringers along the bottom skin at wing stations 60-120).
4) The stringers are oriented so that their long axis is attached via rivets to the top or bottom skins, depending on their location in the wing.
5) In addition to assuming LT type materials, it was assumed that the materials were of A-basis.

Based on these assumptions, it was possible to begin calculating the critical buckling and crippling loads for the stringers. This was done using the following process:

Determine the Slenderness Parameter, B_p

$$B_p = \frac{\frac{b_w}{t_w}}{\sqrt{\frac{KE}{F_{0.7}}}}$$

Where: b_w is the width of the side attached to the skin
t_w is the thickness of the face touching the skin
K is an empirically-derived geometric parameter
E is the compression modulus of elasticity
$F_{0.7}$ is the compression yield load

Using the standard dimensions of a UL #3 extrusion from Military Handbook 5 and Figure 7.12 of Ewing, it was determined that the value of K was .385 (the value of a/b was found to be 11.9, which was well beyond the scope of Figure 7.12 and thus the final value of K for the load case of one side free in compression was assumed). The rest of the variable values could be found in MIL-HNBK-5, and the final value for the slenderness parameter was found to be:

$\boxed{B_p = 1.187}$

Evaluate S_P from "Plate Curve" of Ewing (pg 131)

Once the slenderness parameter was determined, the value of S_P was simply interpreted from Figure 7.8 of Ewing. Using the curve labeled "Plates, Flanges", the value of S_P was found to be:

$$\boxed{S_p \approx 0.80 < 1.0}$$

Since the value of S_P is less than 1.0, the longitudinal member (i.e. the stringer) is unstable and secondary buckling will occur. Based on this observation, the value of the critical buckling stress for secondary buckling had to be determined.

Evaluate B

Before the critical buckling load could be determined, a new value of B had to be calculated based on the assumption that secondary buckling would occur. This was done using the following equation:

$$\boxed{B = \frac{\frac{L'}{\rho}}{\pi\sqrt{\frac{E}{F_{cr^*}}}}}$$

Where: $L' = \frac{L}{\sqrt{c}} = \frac{12}{\sqrt{1.5}} = 9.798in$

$$\rho = \sqrt{\frac{I}{A}} = \sqrt{\frac{.0027in^4}{.0818in^2}} = .18167in$$

$$F_{cr^*} = S_P F_{0.7} = .80(41000psi) = 32800psi$$

Plugging these values into the above equation, along with the value of E_c from the military handbook yields the following:

$$\boxed{B = .950}$$

Determine S_J from "Johnson's Parabola" (Ewing, pg 131)

Using the calculated B value, Figure 7.8 of Ewing can once again be utilized to determine the new S value, which was interpreted visually from the figure. The final value for S_J was as follows:

$$\boxed{S_J \approx .76}$$

Calculate the Critical Buckling Stress, F_{CR}

Once the S_J value has been determined, F_{CR} can be determined using the following equation:

$$\boxed{F_{CR} = S_J F_{CR^*} = S_J S_P F_{0.7} = (.80)(.76)(41000) = 24928psi}$$

Determine Critical Crippling Stress of Stringers Using Goran

The value of the critical crippling stress is determined using the following equation:

$$\frac{Fcc}{Fcy} = \sqrt{\frac{F_{CY}}{E}}\left(\frac{b}{t}\right)$$

Using the previously defined values for each of the variables, the final value of this ratio was calculated to be .7369. Using this ratio and the value of F_{CY}, the calculated value of F_{CC} was found to be as follows:

$$F_{CC} = .7369(41000) = 30213.74 psi$$

Once all of these values were calculated, the FEM was queried for information about the internal loads located in the upper stringers. At each station, inboard, midboard, and outboard, respectively, the critical element of the stringers was evaluated and used for the margin of safety calculation. It was assumed that since the most stressed element is being analyzed, if this element had a positive margin of safety, all other stringer elements in that section of the wing would be acceptable and have positive margins of safety by inspection.

6.6.1 Inboard Wing Section

One of the first analysises conducted on the upper stringer occurred at the inboard section of the wing, which was defined as the section of wing between wing stations 60-120. This section has four stringers along the top skin, all of which should be loaded in compression due to the moment induced by the lift loads. A stress tensor plot was created using PATRAN to aid in identifying the critical element of this section. This tensor can be seen below in Figure 6.1.

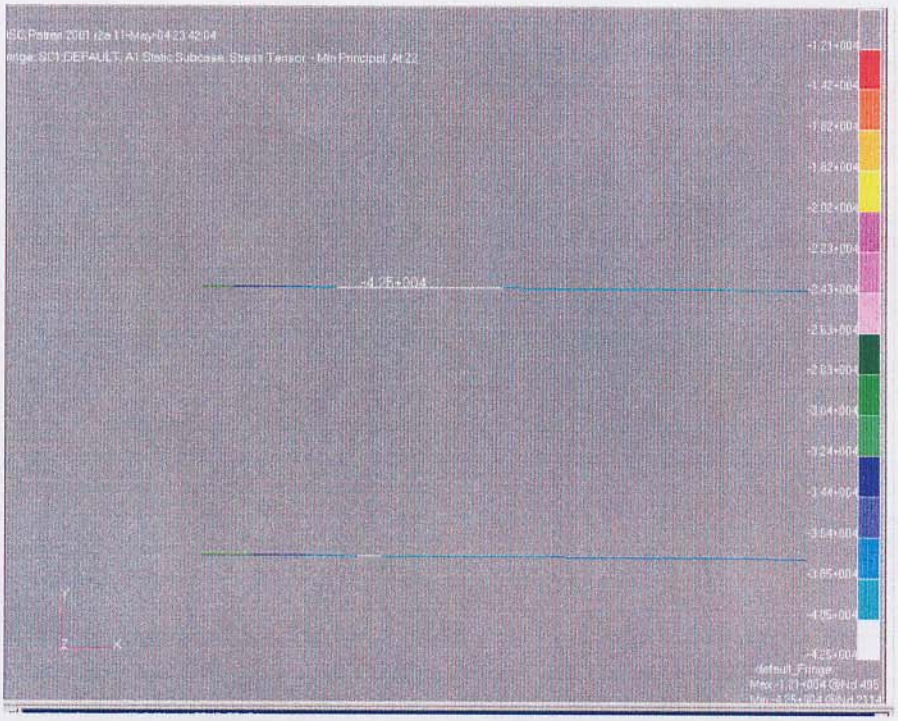

Figure 6.6.1 Stress Tensor of Critical Element of Inboard Upper Stringers

Once the general location of the critical element was determined from the fringe plot of the stress tensor, the PATRAN model was queried for the element identification numbers. This yielded the following:

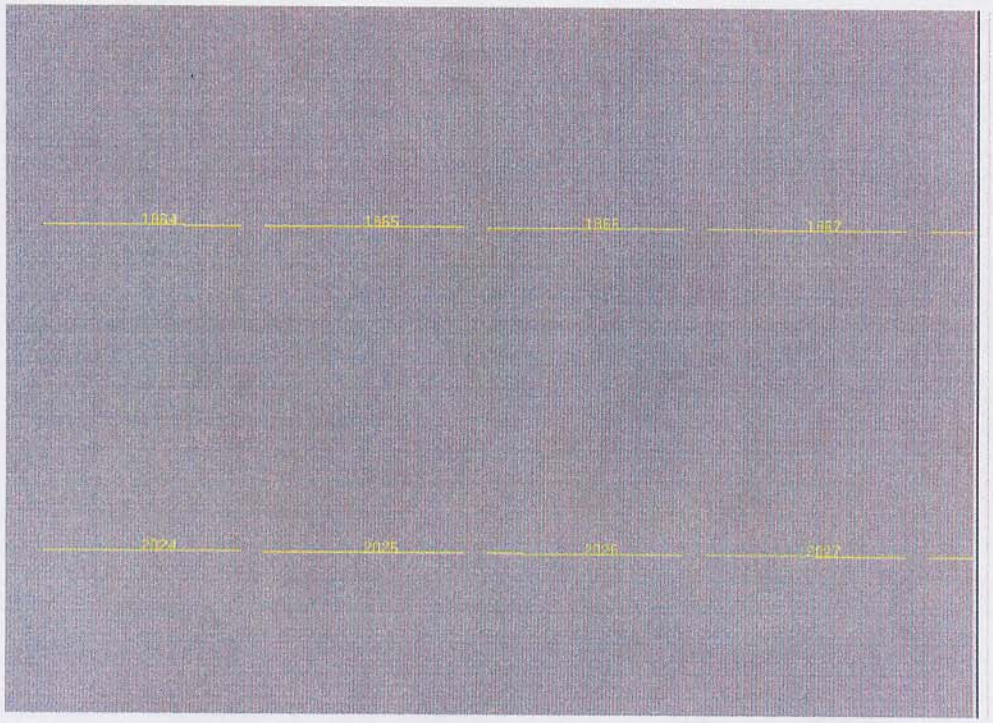

Figure 6.6.2 Upper Inboard Stringer Element Identifications Near Critical Element

Based on the fringe plot of the stress tensor, it was hypothesized that the critical element was either at Element 1864 or Element 1865. The values of the internal stresses were determined using the .f06 file, which resulted in the following data:

SUBCASE

STRESSES IN BEAM ELEMENTS (CBEAM)

ELEMENT-ID	GRID	STAT DIST/ LENGTH	SXC	SXD	SXE	SXF	S-MAX	S-MIN
	303	0.000	[illegible]	[illegible]	[illegible]	[illegible]	2.041814E+04	-5.117716E+04
	2114	1.000	-1.218632E+04	-4.336982E+04	-3.004205E+04	-1.084288E+04	-1.084288E+04	-4.336982E+04
1865								
	2114	0.000	-4.422307E+03	-3.728964E+04	-4.627600E+04	-5.328131E+03	-4.422307E+03	-4.627600E+04
	2115	1.000	-2.309747E+04	-4.040992E+04	-3.242201E+04	-2.229229E+04	-2.229229E+04	-4.040992E+04
1866								
	2115	0.000	-1.850825E+04	-3.655175E+04	-4.262092E+04	-1.912002E+04	-1.850825E+04	-4.262092E+04
	2116	1.000	-2.731934E+04	-3.893481E+04	-3.562347E+04	-2.698555E+04	-2.698555E+04	-3.893481E+04
1867								
	2116	0.000	-2.524313E+04	-3.731920E+04	-3.994147E+04	-2.550746E+04	-2.524313E+04	-3.994147E+04
	2117	1.000	-2.802038E+04	-3.813047E+04	-3.770545E+04	-2.797754E+04	-2.797754E+04	-3.813047E+04
1868								
	2117	0.000	-2.784160E+04	-3.794146E+04	-3.819125E+04	-2.786678E+04	-2.784160E+04	-3.819125E+04
	2118	1.000	-2.687005E+04	-3.765447E+04	-3.897509E+04	-2.700317E+04	-2.687005E+04	-3.897509E+04
1869								
	2118	0.000	-2.777621E+04	-3.837891E+04	-3.704623E+04	-2.764187E+04	-2.764187E+04	-3.837891E+04
	2119	1.000	-2.435578E+04	-3.734413E+04	-3.981813E+04	-2.460516E+04	-2.435578E+04	-3.981813E+04
1870								
	2119	0.000	-2.606838E+04	-3.872635E+04	-3.614262E+04	-2.580793E+04	-2.580793E+04	-3.872635E+04
	2120	1.000	-2.037733E+04	-3.735673E+04	-4.057641E+04	-2.070187E+04	-2.037733E+04	-4.057641E+04
1871								
	2120	0.000	-2.262838E+04	-3.916069E+04	-3.577415E+04	-2.228701E+04	-2.228701E+04	-3.916069E+04
	325	1.000	-1.467350E+04	-3.888755E+04	-4.114093E+04	-1.490064E+04	-1.467350E+04	-4.114093E+04
1872								
	325	0.000	-1.537051E+04	-3.860141E+04	-3.952907E+04	-1.546402E+04	-1.537051E+04	-3.952907E+04
	2123	1.000	-1.945282E+04	-3.794377E+04	-3.717873E+04	-1.937570E+04	-1.937570E+04	-3.794377E+04
1873								
	2123	0.000	-1.915671E+04	-3.767398E+04	-3.788472E+04	-1.917796E+04	-1.915671E+04	-3.788472E+04
	2124	1.000	-2.071968E+04	-3.706086E+04	-3.716775E+04	-2.073045E+04	-2.071968E+04	-3.716775E+04
1874								
	2124	0.000	-2.092128E+04	-3.714816E+04	-3.690807E+04	-2.089707E+04	-2.089707E+04	-3.714816E+04
	2125	1.000	-2.098867E+04	-3.646436E+04	-3.720988E+04	-2.106382E+04	-2.098867E+04	-3.720988E+04
1875								
	2125	0.000	-2.150034E+04	-3.686200E+04	-3.614665E+04	-2.142823E+04	-2.142823E+04	-3.686200E+04
	2126	1.000	-2.071501E+04	-3.595744E+04	-3.712066E+04	-2.083226E+04	-2.071501E+04	-3.712066E+04
1876								
	2126	0.000	-2.151139E+04	-3.656020E+04	-3.550288E+04	-2.140481E+04	-2.140481E+04	-3.656020E+04
	2127	1.000	-2.021265E+04	-3.547919E+04	-3.690364E+04	-2.035624E+04	-2.021265E+04	-3.690364E+04

1 MSC.NASTRAN JOB CREATED ON 07-MAY-04 AT 06:13:40 MAY 11, 2004 MSC.NASTRAN 6/11/01

Figure 6.6.3 .F06 Data Near Critical Element in Upper Inboard Stringers

As can be seen from Figure 6.33, there were numerous data points collected at each node, with PATRAN calculating four different stress values for four different points along the cross section of the stringer. The location of these data points can be seen in Figure 6.34 below.

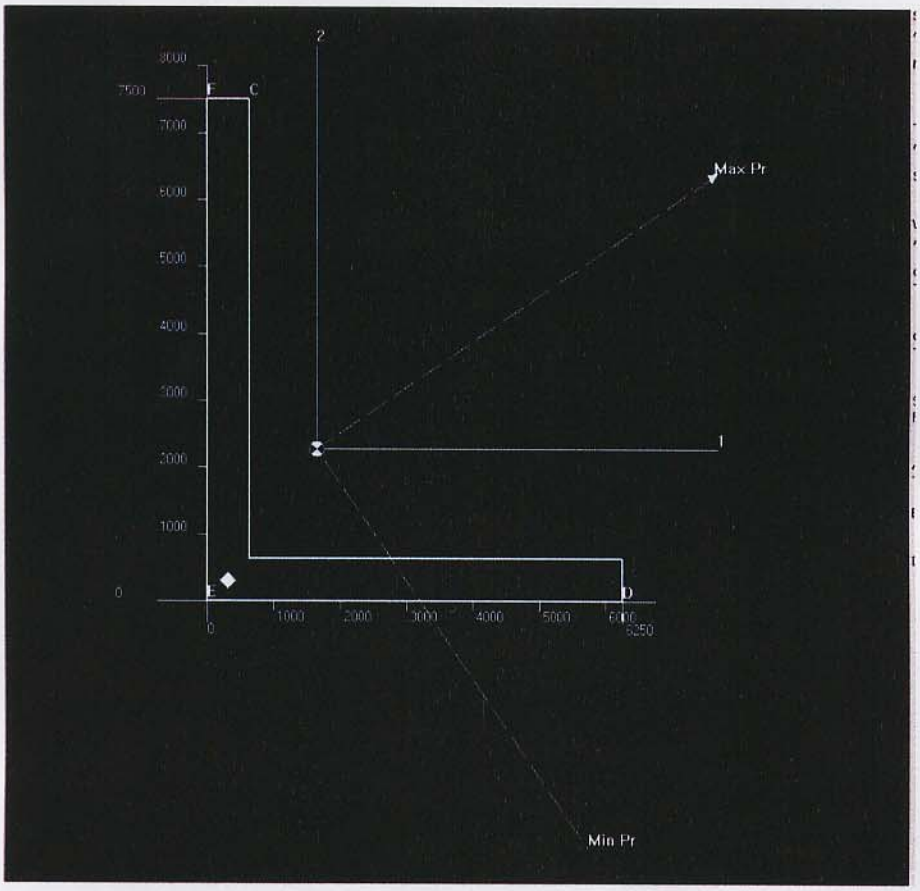

Figure 6.6.4 PATRAN .f06 Data Value Locations

It should also be noted that for this section of the wing, there is definitely a anomolus series of data points due to the presense of boudnary conditions where the boom mates to the wing. These boundary conditons restricted the degree of freedom in the local z-direction, which in turn influcenced the stiffness matrix and the resultant stresses and strains of the model. This was very apparent with the calculated values of stress at Element 1864, where some of the calculated stresses indicated tension loading, even though the member is in compression. This type of error had to be accounted for during the analysis of the model.

Additionaly, it is obvious that two distinct values are needed for the margin of safety calculations: a buckling stress value and a crippling stress value. At this point, an analysis paradigm was created in which the actual buckling stress would be defined as the average stress values of points F,C,E, and D and the actual crippling stress value would be the average of the stress values at points F, C, and E. This paradigm was considered accepatable for the following reasons:

1) This is a very conservative assumption. By averaging the values of the most highly stressed element and using it for the margin of safety calculations, a positive margin of safety would mean that not only is the entire section of the wing acceptable, it is also heavy.
2) Since loads on all points of the cross section can have an effect on the buckling behavior of the beam, all data points should be included to maintain conservative analysis.

3) Since the stringers are connected to the skins through rivets, the stringers can be assumed to be supported throughout their length. This makes any buckling analysis extremely conservative.
4) The method through which the crippling load is calcualated is also highly convservative in that it only accounts for the stringer itself. In a real world dynamic model, crippling of the stringers would also depend on the crippling and buckling behavior of the surrounding skins, webs, spar caps, and ribs. Since these events are not considered (and since they may greatly reduce the crippling load on the stringer), the crippling estimate is very conservative.
5) The crippling event will occur along the the face of the cross section that is connected to the skin. Therefore, any stresses on that face would carry more influence on the crippling behavior of the member then a stress on the face with one edge free. It is therefore acceptable to disregard the stress calcualted at point D due to its location on the cross section.

With this analysis paradigm in mind, the stresses in Element 1864 (the critical element) were used to determine the buckling and crippling stresses at the critical member. This analysis yielded the following stress values:

Buckling Stress	Crippling Stress
-47564.75 psi	-51177.16 psi

Note: According the moment theory, this element should have the highest stresses in compression (which is why this element was chosen as the critical element of the upper stringers). However, the values of the stresses acting on this element are being greatly influenced by the nearby boundary conditions located at the intersection between the boom and the wing. The presence of these displacement limiations influences the stiffness at the nodes of the element, which in turn affects the forces and stresses that are calculated for that element. In this case, two of the calculated stress values were found to be positive (i.e. tensile loading). Since these values are most likely erroneous, only the compressive stress values were used in determining the buckling and crippling stresses of the critical element. Since the maximum compressive values of stress were used, it was assumed that this analysis decision was conservative enough to be considered justifiable.

6.6.2 Mid Wing Section

A similar analysis process was used to find the stresses on the critical element of the midboard section of the wing. The stress tensor plot of the upper, midboard section of the stringers is shown on the next page. By inspection, it is apparent that the maximum stresses are occuring at the most inboard section of the wing section near the leading edge spar, where most of the lift load is being applied. It is also appearant that maximum compressive stress of this fringe plot is lower then that of the inboard section of the wing. Both of these phenomena were expected.

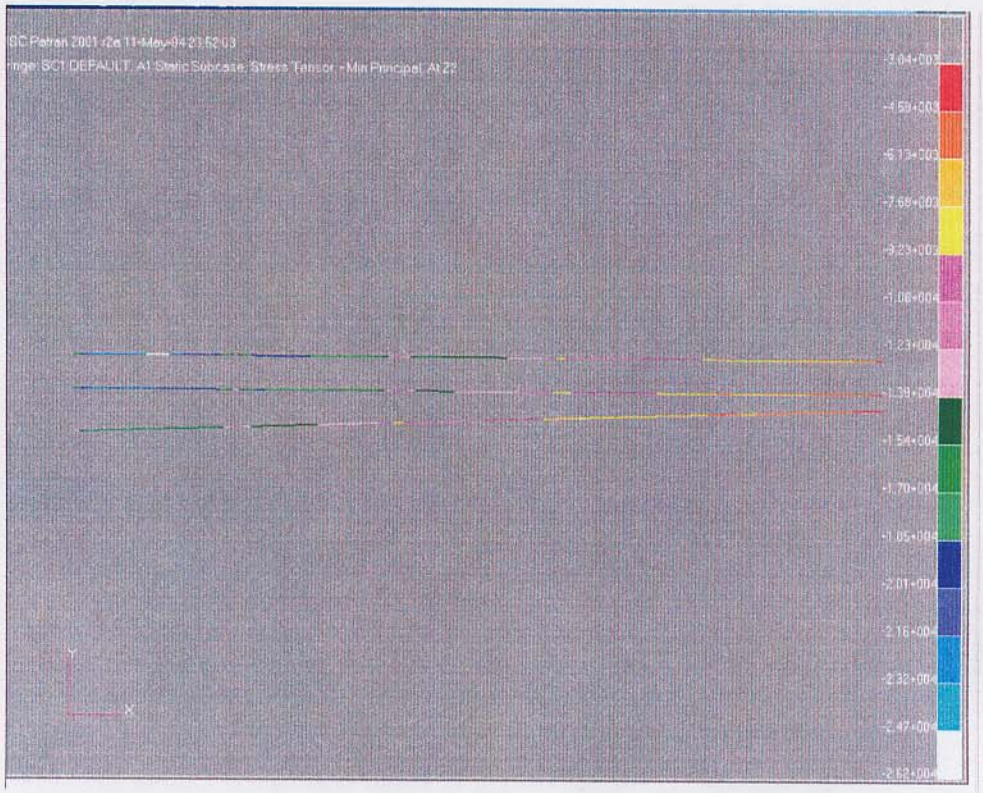

Figure 6.6.5 PATRAN Stress Tensor Fringe Plot of Upper, Midboard Stringers

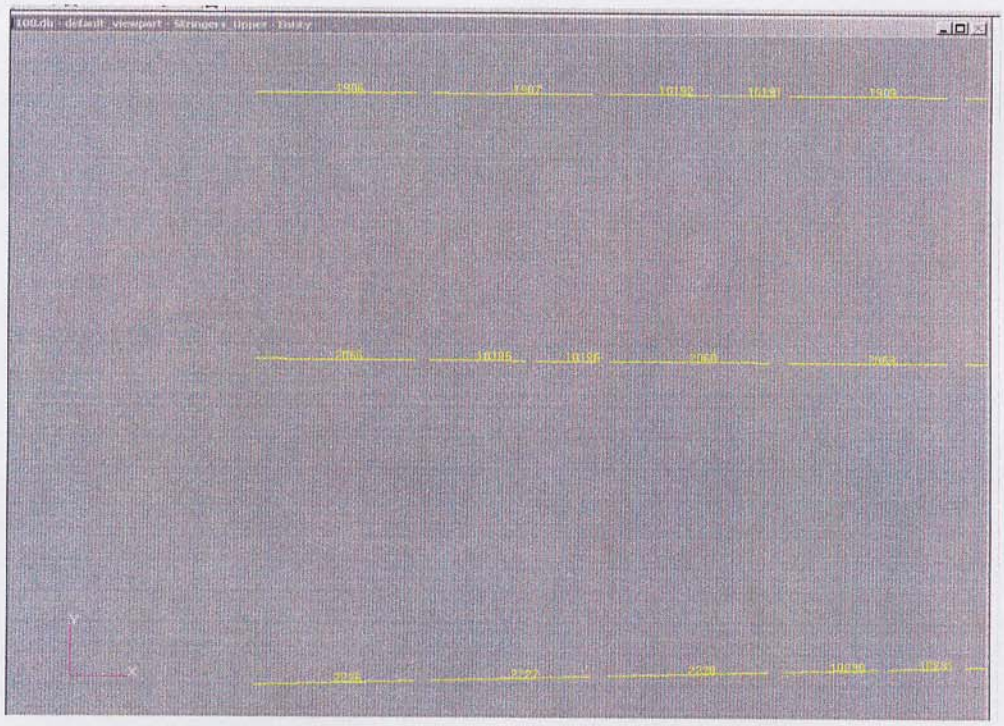

Figure 6.6.6 PATRAN Element Identification of Critical Element in Upper, Midboard Stringers

(Element 1906 = Local Critical Element)

S T R E S S E S I N B E A M E L E M E N T S (C B E A M)

	ELEMENT-ID	GRID	STAT DIST/ LENGTH	SXC	SXD	SXE	SXF	S-MAX	S-MIN	M.S.-T	M.S.-C
0	1902										
		2155	0.000	-1.305912E+04	-2.515542E+04	-2.396286E+04	-1.293891E+04	-1.293891E+04	-2.515542E+04		
		2156	1.000	-1.167465E+04	-2.416265E+04	-2.537532E+04	-1.179688E+04	-1.167465E+04	-2.537532E+04		
0	1903										
		2156	0.000	-1.249699E+04	-2.481724E+04	-2.362781E+04	-1.237709E+04	-1.237709E+04	-2.481724E+04		
		489	1.000	-1.102940E+04	-2.460770E+04	-2.469848E+04	-1.103855E+04	-1.102940E+04	-2.469848E+04		
0	1904										
		489	0.000	-1.148261E+04	-2.407611E+04	-2.361979E+04	-1.143661E+04	-1.143661E+04	-2.407611E+04		
		2159	1.000	-1.136347E+04	-2.316671E+04	-2.415837E+04	-1.146343E+04	-1.136347E+04	-2.415837E+04		
0	1905										
		2159	0.000	-1.215025E+04	-2.375469E+04	-2.257690E+04	-1.203153E+04	-1.203153E+04	-2.375469E+04		
		2160	1.000	-1.120495E+04	-2.223779E+04	-2.396597E+04	-1.137915E+04	-1.120495E+04	-2.396597E+04		
0	1906										
		2160	0.000	-1.276608E+04	-2.343031E+04	-2.076746E+04	-1.249766E+04	-1.249766E+04	-2.343031E+04		
		2161	1.000	-1.092981E+04	-1.960149E+04	-2.391229E+04	-1.136434E+04	-1.092981E+04	-2.391229E+04		
0	1907										
		2161	0.000	-1.693038E+04	-2.422468E+04	-1.152530E+04	-1.565029E+04	-1.152530E+04	-2.422468E+04		
		2162	1.000	-3.153920E+03	8.517951E+03	-3.715238E+04	-7.757490E+03	8.517951E+03	-3.715238E+04		
0	1909										
		2163	0.000	-8.426161E+03	-8.596246E+03	-2.642210E+04	-1.022301E+04	-8.426161E+03	-2.642210E+04		
		2164	1.000	-1.272932E+04	-2.165179E+04	-1.698588E+04	-1.225899E+04	-1.225899E+04	-2.165179E+04		
0	1910										
		2164	0.000	-1.120086E+04	-2.037939E+04	-2.036107E+04	-1.119902E+04	-1.119902E+04	-2.037939E+04		
		2165	1.000	-1.006392E+04	-2.048649E+04	-2.105415E+04	-1.012114E+04	-1.006392E+04	-2.105415E+04		
0	1911										
		2165	0.000	-1.041782E+04	-2.074553E+04	-2.035597E+04	-1.037855E+04	-1.037855E+04	-2.074553E+04		
		460	1.000	-9.644006E+03	-2.092409E+04	-2.077420E+04	-9.628897E+03	-9.628897E+03	-2.092409E+04		
0	1912										
		460	0.000	-1.015417E+04	-2.051976E+04	-1.976557E+04	-1.007815E+04	-1.007815E+04	-2.051976E+04		
		2168	1.000	-9.389163E+03	-1.979096E+04	-2.063726E+04	-9.474471E+03	-9.389163E+03	-2.063726E+04		
0	1913										
		2168	0.000	-1.006350E+04	-2.033514E+04	-1.918554E+04	-9.947615E+03	-9.947615E+03	-2.033514E+04		
		2169	1.000	-8.853227E+03	-1.932259E+04	-2.049350E+04	-8.971255E+03	-8.853227E+03	-2.049350E+04		
0	1914										
		2169	0.000	-9.723865E+03	-1.997672E+04	-1.873513E+04	-9.598712E+03	-9.598712E+03	-1.997672E+04		
		2170	1.000	-8.410733E+03	-1.888582E+04	-2.015036E+04	-8.538199E+03	-8.410733E+03	-2.015036E+04		
0	1915										

1 MSC.NASTRAN JOB CREATED ON 07-MAY-04 AT 06:13:40 MAY 11, 2004 MSC.NASTRAN 6/11/01 PAGE 1518
DEFAULT

Figure 6.6.7 .F06 File Data of Critical Element Stresses (Element 1906)

Using the data from the .f06 file and the analysis paradigm, the following local bending and crippling stresses were found for Element 1906, the local critical element.

Buckling Stress	Crippling Stress
-17365.26 psi	-15343.71 psi

6.6.3 Outboard Wing Section

A similar analysis process was used to find the stresses on the critical element of the midboard section of the wing. The stress tensor plot of the upper, outboard section of the stringers is shown on the next page. By inspection, it is apparent that the maximum stresses are occurring at the most inboard section of the wing section near the leading edge spar, where most of the lift load is being applied. It is also apparent that maximum compressive stress of this fringe plot is lower then that of the inboard and midboard sections of the wing. Both of these phenomena were expected.

Figure 6.10.10 Area of Shear Interest for Rib Rivet Shear

The black square shown on the two figures (previous and following) corresponds to the same element and its positioning.

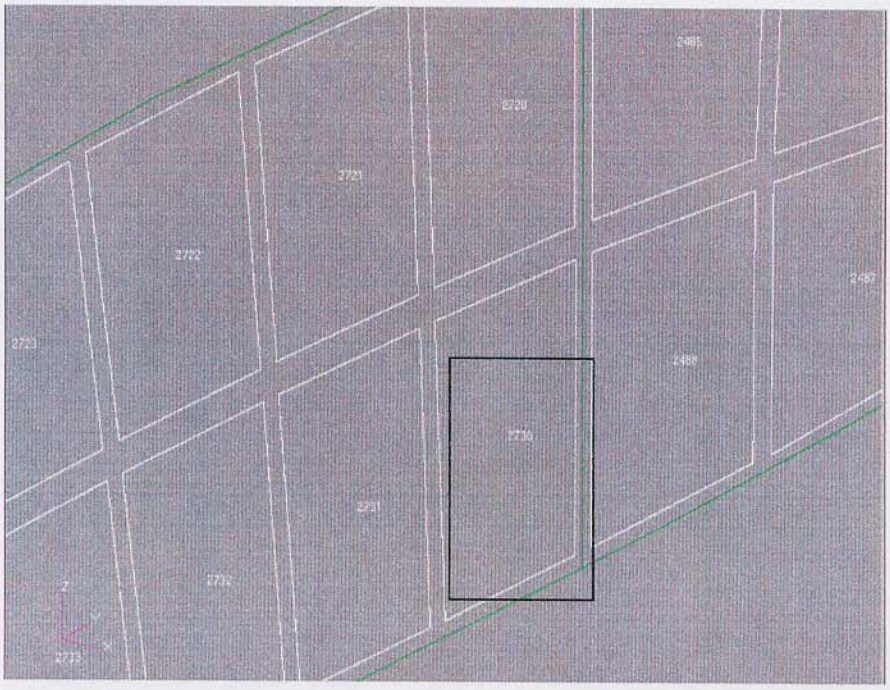

Figure 6.10.11 Critical Element for Shear Interest of Rivet Shear (WS 60 Rib) #2730

The .f06 output for the element stress of Element 2730 is given in the following figure. It should be noted that the centroid value of the *GRID-ID* was used and that the values of merit are the *MAJOR* and *MINO*R stress values at zero shear because the maximum limit shear is determined from these values (as seen from the equation shown in the calculation procedure section).

S T R E S S E S I N Q U A D R I L A T E R A L E L E M E N T S (Q U A D 4) OPTION = BILIN

ELEMENT ID	GRID-ID	FIBER DISTANCE	STRESSES IN ELEMENT COORD SYSTEM NORMAL-X	NORMAL-Y	SHEAR-XY	PRINCIPAL STRESSES (ZERO SHEAR) ANGLE	MAJOR	MINOR	VON MISES
2730	CEN/4	-1.600000E-02	-3.719032E+03	-1.500518E+03	3.607978E+03	53.5449	1.164871E+03	-6.384421E+03	7.039516E+03
		1.600000E-02	-3.637339E+03	-8.633024E+02	3.522172E+03	55.7472	1.535114E+03	-6.035755E+03	6.931990E+03
	2747	-1.600000E-02	-1.722013E+03	-1.488102E+03	3.485191E+03	45.9610	1.882096E+03	-5.092210E+03	6.249554E+03
		1.600000E-02	-1.538748E+03	-9.491342E+02	3.396471E+03	47.4804	2.165300E+03	-4.653183E+03	6.034582E+03
	3288	-1.600000E-02	-1.781911E+03	-1.498051E+03	3.489197E+03	46.1647	1.852101E+03	-5.132063E+03	6.266854E+03
		1.600000E-02	-1.601473E+03	-7.628557E+02	3.394041E+03	48.5214	2.237680E+03	-4.602008E+03	6.040158E+03
	313	-1.600000E-02	-5.709848E+03	-1.513270E+03	3.730395E+03	59.6785	6.684717E+02	-7.891589E+03	8.246171E+03
		1.600000E-02	-5.729401E+03	-7.705695E+02	3.647240E+03	62.1040	1.160215E+03	-7.660186E+03	8.301325E+03
	65	-1.600000E-02	-5.769723E+03	-1.502953E+03	3.733716E+03	59.8715	6.638905E+02	-7.936567E+03	8.288478E+03
		1.600000E-02	-5.792568E+03	-9.730214E+02	3.657929E+03	61.6881	9.975540E+02	-7.763144E+03	8.306965E+03

Figure 6.10.12 .F06 Output Stresses in Element 2730

6.10.4 Margins of Safety and Rivet Design

The following two tables summarize the rivet design as well as corresponding margins of safety of the design. All calculations used to obtain these values were done by hand and are located in Appendix A.

Table 6.10.1 Final Fastener (Rivet) Design

Rivet Design						
	Material	**Diameter**	**Type**	**Spacing**	**Pitch**	**e/D**
Skin	2024-T31 Aluminum	1/8"	Protruding Head	3/16"	0.5"	2.0
Web	2024-T31 Aluminum	1/8"	Protruding Head	0.5"	---	2.0
Ribs	2024-T31 Aluminum	1/8"	Protruding Head	1.0"	---	2.0

Table 6.10.2 Margins of Safety for Fastener Design

Margins of Safety (MS)			
	Skin	*Web*	*Ribs*
Rivet Shear	0.26	0.13	2.21
Sheet Bearing	0.32	0.87	0.78

Conclusion of Design and Analysis

As seen by the design, it is required for the skin to actually have two rows of rivets rather than just one row, and this is due to the restriction that 1/8" protruding head rivets must be spaced at 0.5" at minimum. Knowing that the spar caps are UL#6 with the longer leg flush to the skins, there is no worry in the fitting of the rivets. Yet, the stringers are UL#3, which make for a very tight fit at the radial corner where the two legs of the extrusion meet. It is unacceptable for rivets to be bucked and end up interfering with this radial corner. Therefore, to avoid this possibility within manufacturing tolerances, a good solution would be to either choose a different (and longer-legged) extrusion or to increase the diameter size of the rivets one or two standard sizes higher than what it is currently – this would lead to having to possibly worry about sheet bearing failure though.

6.11 Verification of FEM Results

One important and simple check to assure whether or not the FEM model (using PATRAN) is operating with the loads one defines is to look at the resultant loads. In the figure below, it shows that there is no reaction load along the x-direction (T1), a drag force of -242.1 lbs in the y-direction (T2), and a lift force of 2411 lbs in the z-direction (T-3). The second figure shows the orientation of the wing frame relative to a global coordinate system. Notice that these values are the same as with what was defined in section 5.3.

```
                                E L E M E N T   G E O M E T R Y   T E S T   R E S U L T S   S U M M A R Y
                                              TOTAL NUMBER OF TIMES TOLERANCES WERE EXCEEDED
                                    ASPECT/       MINIMUM       MAXIMUM      SURFACE/FACE                              EDGE POINT     JACOBIAN
      ELEMENT TYPE   SKEW ANGLE   TAPER RATIO  INTER. ANGLE  INTER. ANGLE   WARP FACTOR   OFFSET RATIO  LENGTH RATIO  DETERMINANT
          BAR            N/A          N/A           N/A           N/A           N/A             0            N/A           N/A
          BEAM           N/A          N/A           N/A           N/A           N/A             0            N/A           N/A
          QUAD4            0            2             0            40             0           N/A            N/A           N/A
          TRIA3            0          N/A           N/A             0           N/A           N/A            N/A           N/A

          N/A IN THE ABOVE TABLE INDICATES TESTS THAT ARE NOT APPLICABLE TO THE ELEMENT TYPE AND WERE NOT PERFORMED.
          FOR ALL ELEMENTS WHERE GEOMETRY TEST RESULTS HAVE EXCEEDED TOLERANCES,

          QUAD4     ELEMENT ID     7249 PRODUCED LARGEST  TAPER RATIO      OF       0.53 (TOLERANCE =       0.50).
          QUAD4     ELEMENT ID     2999 PRODUCED LARGEST  INTERIOR ANGLE   OF     157.15 (TOLERANCE =     150.00).
1     MSC.NASTRAN JOB CREATED ON 07-MAY-04 AT 06:13:40                              MAY  10, 2004  MSC.NASTRAN  6/11/01   PAGE     7

0
 *** USER INFORMATION MESSAGE 7310 (VECPRN)
     ORIGIN OF SUPERELEMENT BASIC COORDINATE SYSTEM WILL BE USED AS REFERENCE LOCATION.
     RESULTANTS ABOUT ORIGIN OF SUPERELEMENT BASIC COORDINATE SYSTEM IN SUPERELEMENT BASIC SYSTEM COORDINATES.
0                                                    OLOAD     RESULTANT
  SUBCASE/    LOAD
  DAREA ID    TYPE          T1             T2             T3             R1             R2             R3
0       1     FX    0.000000E+00          ----           ----           ----    0.000000E+00   0.000000E+00
              FY           ----   -2.420800E+02          ----    1.535681E+02          ----   -2.762206E+04
              FZ           ----          ----    2.411120E+03   -2.103832E+04   -2.751164E+05          ----
              MX           ----          ----           ----    0.000000E+00          ----           ----
              MY           ----          ----           ----           ----    0.000000E+00           ----
              MZ           ----          ----           ----           ----          ----    0.000000E+00
            TOTALS  0.000000E+00  -2.420800E+02   2.411120E+03   -2.088476E+04   -2.751164E+05  -2.762206E+04
1     MSC.NASTRAN JOB CREATED ON 07-MAY-04 AT 06:13:40                              MAY  10, 2004  MSC.NASTRAN  6/11/01   PAGE     8
```

Figure 6.11.1 .F06 Verification of External Loads

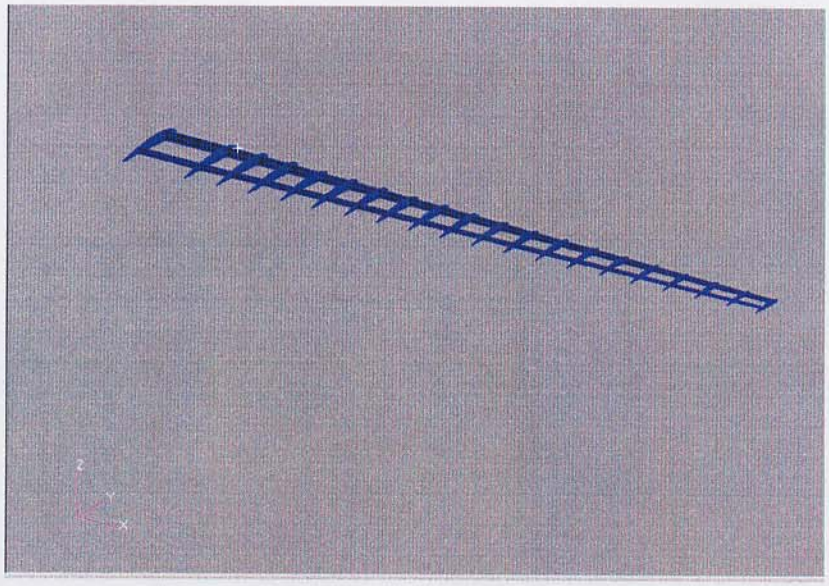

Figure 6.11.2 Guts of Wing Showing Wing Geometry Orientation

The entire idea behind the method of finite element modeling is to basically linearize the reaction of an element about the number of its surrounding nodes, which each has 6 degrees of freedom in 3-D space (3 translational and 3 rotational), and to take a known quantity (either force(s) or displacement(s)) acting on the element(s) and to extract the unknown of those two quantities. This is done by creating a stiffness matrix, [k], which is representative of the type of element being modeled (or combination of elements such as the wing of this project). The stiffness matrix associated with either the known force(s) or displacement(s) allows one to solve for the unknown matrix of values using the equation below, where [F] is the force matrix, [k] is the stiffness matrix, and [q] is the displacement matrix.

$$[F] = [k][q]$$

The most important characteristic to realize about finite element modeling is that answers are never discrete. The reactions at individual nodes will be correct based on a correctly developed model, but because the entire system (of elements) is linearized, stress and/or force values based on non-linear distributions (i.e. pressures, temperatures, loadings, moments) acting on the model given within an .f06 output for elements between the nodes will not be exactly accurate – the more elements spanning between two node locations, the more accurate the model and stress/force values become.

The validity of a PATRAN FEM model can be determined by a value named "epsilon" (strain energy value), which is defined in the .f06 file ran by NASTRAN. Basically, the epsilon value numerically indicates whether the PATRAN program believes its own results. In the case where singular matrices occur within the program, the epsilon value is driven away from zero (where zero represents perfect results based on the model creation). The epsilon value found from the model used for this analysis was on the order of a -constant x 10^12. In general practice, this would be unacceptable, yet after talking with Dr. Richard Hale, Associate Professor at The University of Kansas, he claimed that it could be due to the sharp angle turn associated with the leading edge elements of the model (see figure below). Because the leading edge was not of particular concern within this analysis, the skewed value of epsilon was treated as if it were within reason for the type of mesh element created at the front leading edge.

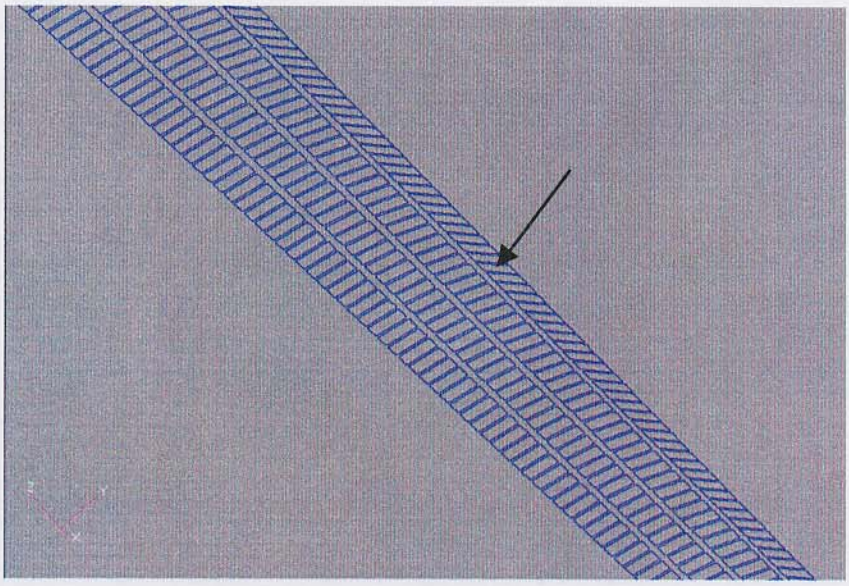

Figure 6.11.3 Sharp Leading Edge Discontinuity for Leading Edge Element Surface

Even if the value for epsilon is extremely close to zero, it does not necessarily mean that the model results are completely accurate. A well defined mesh for surfaces consists of square shaped quadrilateral elements (i.e. – aspect ratio of 1) throughout the surface. The more skewed the aspect ratio becomes, then the worse the results in the .f06 results file. For an odd shaped surface such as the skin surfaces of a tapered and cambered wing, there is a definite likelihood that quadrilateral elements will have poorer aspect ratios at some point along the wing surface and in some cases, triangle elements must be used in order to meet nodal continuity between elements (using triangle elements gives a very poor representation of what should truly be happening in the model). Because a model is easily subject to a poor representation of how the actual object behaves given as set of load or boundary conditions, discretizations should be run to find convergence in the results. The gives a nice "warm fuzzy" inside and lets one know that the model is nearing theoretical perfection.

Unfortunately, there was not enough time to discretize the model for this analysis. Therefore, all numbers are based on the original model produced.

7.0 Conclusions

7.1 Validity of the design

Based on the analysis of the internal stresses in the ribs, skins, spars, stringers, webs, and flanges taken from the .f06 file of the PATRAN model, the following conclusions were made:

1) The top skin was insufficient to take the limit loads applied to the structure.
2) The critical element of the top stringers failed in both buckling and crippling near the boundary condition of the inboard wing section.
3) The load not carried by these elements would have to be transferred to other wing structure elements, such as the stringers, the spar caps, or the ribs. This in turn could cause the previously calculated positive margins of safety to become negative in a series of progressive, "trickle down" failures.
4) In addition to these failed elements, there were also some elements with excessively large margins of safety, which in turn is an unnecessary increase in structural weight.
5) Throughout the model, extremely conservative assumptions were made. For example, a rectangular lift distribution along the spars would cause the moment arm of the distributed force to approach the center of wing, which in turn increases the applied moment at the inboard section where negative margins of safety were observed. In a more realistic distribution of load, the load distribution would be elliptical or somewhat triangular, which would bring the moment arm closer to the inboard section of the wing. This in turn would reduce the moment induced at this section of the wing and could cause the negative margin of safety values to become less negative (or even positive). Also, the average of the maximum stresses of the shell elements were used in the margin of safety calculations. This implies that the wing is much more heavily stressed then the model is reporting, which is inherently very conservative.

7.2 Recommendations for Further Analysis

1) A more realistic external load distribution should be formulated for a more accurate model response.
2) Model the boom in terms of forces and torques acting on the wing at the corresponding wing station locations.
3) Perform a convergence study on the model to demonstrate model accuracy.
4) Increase the meshing at the critical stress locations for more accurate critical element stress values.
5) Correct the alignment and offsets of all errant longitudinals.
6) Work to improve the aspect ratio of the quad elements and work to ensure that there are as few triangular elements as possible.
7) Investigate the effects of wing deflection and angle of twist on the wing on load cases and aircraft predicted performance.
8) Investigate optimization strategies.
9) Model cases where negative load factors are experienced.

7.3 Recommendations for Design Modifications

1) Change the material type of the stringers to 7075-T6 aluminum extrusions (higher allowable loads, little weight penalty).
2) Institute a three-spar concept, with another spar along the leading edge on the opposite side of the spar web from the original leading edge spar. This will reduce overall wing deflection and make the wing more resistant to twist.